# Three-Dimensional Simulations of Ion Acceleration from a Foil Irradiated by a Short-Pulse Laser

A. Pukhov

*Max-Planck-Institut für Quantenoptik, Hans-Kopfermann-Strasse 1, 85748 Garching, Germany*
(Received 21 November 2000)

Using 3D particle-in-cell simulations we study ion acceleration from a foil irradiated by a laser pulse at $10^{19}$ W/cm$^2$ intensity. At the front side, the laser ponderomotive force pushes electrons inwards, thus creating the electric field by charge separation, which drags the ions. At the back side of the foil, the ions are accelerated by space charge of the hot electrons exiting into vacuum, as suggested by Hatchett *et al.* [Phys. Plasmas **7**, 2076 (2000)]. The transport of hot electrons through the overdense plasma and their exit into vacuum are strongly affected by self-generated magnetic fields. The fast ions emerge from the rear surface in cones similar to those detected by Clark *et al.* [Phys. Rev. Lett. **84**, 670 (2000)].

Recent experiments in which high-intensity laser pulses interact with solid targets have revealed highly collimated beams of multi-MeV ions emerging from the rear surface of the target [1–3]. Roth *et al.* [4] have proposed a new approach to fast ignition of inertial confinement fusion targets that exploits these ion beams. In this context, the detailed understanding of the ion acceleration from laser irradiated solids is of primary interest. Up to now, two different mechanisms have been proposed to explain the experimentally observed high-energy ions.

The first explanation is that the ions are accelerated at the front surface and propagate through the target [3]. If this is true, one would get a unique and very powerful tool for diagnosing self-generated fields inside the solid state body. Indeed, these fields will change the ion energies and propagation direction. Thus, analyzing energy and angular distribution of the emerging ions one could restore the full fields distribution. However, for this diagnostic to be useful, one must know initial parameters of the generated ion beam such as the angular spread and the energy spectrum.

The second explanation is that the ions are accelerated at the rear surface of the target [1,2]. In this case electrons heated by the laser at the front surface of the target propagate through the solid material and form a space charge cloud in vacuum at the rear surface. The static electric field induced by this electron cloud is strong enough to ionize the material and accelerate ions perpendicularly to the rear surface up to multi-MeV energies. This may provide a useful mechanism for generation of high-intensity low-emittance ion beams with various applications envisioned. This mechanism depends crucially on laser conversion into hot electrons and their propagation dynamics inside the target. As the electron currents in question may reach mega-ampere values, the propagation dynamics is strongly influenced by self-generated magnetic fields [5–7]. This electron dynamics is highly nonlinear and needs detailed investigation.

Here we present three-dimensional (3D) particle-in-cell (PIC) simulations of a model problem using the code VLPL (the Virtual Laser Plasma Laboratory) [8]. A laser pulse of wavelength $\lambda = 1$ $\mu$m and maximum intensity $I_0 = 10^{19}$ W/cm$^2$ is incident on a plasma layer of density $n = 16n_c$, where $n_c = \pi mc/\lambda e^2$ is the critical electron density. The laser pulse has a Gaussian profile in time and space: $I = I_0 \exp[-(t - t_0)^2/\tau^2] \exp(-r^2/r_0^2)$, the time duration $\tau = 150$ fs, and the focal spot radius $r_0 = 5.6$ $\mu$m. The peak of the laser pulse reaches the simulation box $t_0 = 150$ fs after the simulation starts. The overdense plasma layer is 12 $\mu$m thick preceded by a ramp where the density rises linearly from 0 to $n$ over a distance of 7.5 $\mu$m. This density gradient models the preplasma usually present in high-intensity laser-solid interactions. We also introduce an exponential density gradient at the rear surface with scale length $L_r = 0.5$ $\mu$m. The full simulation box has size $X \times Y \times Z = 32 \times 40 \times 40$ $\mu$m$^3$. The laser propagates in the $X$ direction. The simulation box is sampled by a grid of $1024 \times 80 \times 80$ cells. The lateral boundary conditions are periodic. The front boundary radiates the laser beam, while both front and back boundaries absorb outgoing radiation and particles. There is a vacuum gap of 15 $\mu$m between the rear surface of the plasma and the back boundary of the simulation box. This space allows for ion acceleration by plasma expansion into vacuum. We should mention that the maximum electron density in the plasma slab, the size of our simulation box, and the laser duration are limited by computer capabilities and differ from usual experimental parameters. In this sense, we present a "model" simulation. It has been performed on 128 processors of CRAY-T3E at Rechenzentrum Garching. The run took 24 hours.

The ion energy spectra we observe in our simulation are shown in Fig. 1. The three curves correspond to ions accelerated at the front plasma surface by the laser ponderomotive push (marked by filled triangles), ions extracted from the rear surface (open circles), and the selection of ions which would hit an ion spectrometer with 2° acceptance angle placed normally to the rear plasma surface (filled circles). Now, we proceed in discussing the mechanisms of ion acceleration.
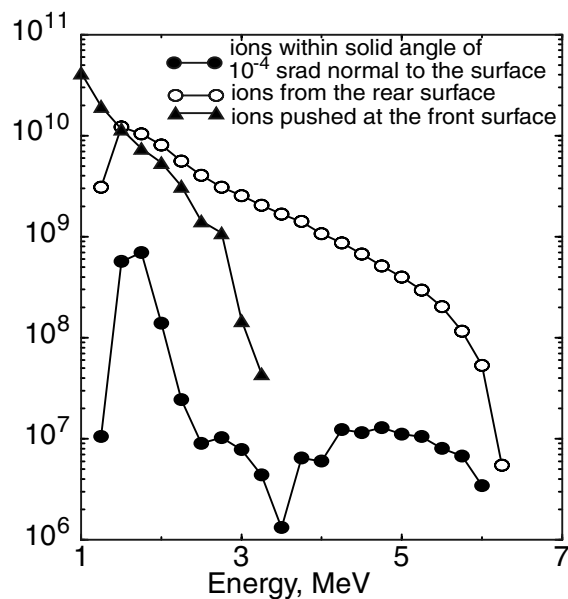
FIG. 1.   Ion energy spectra. The lines represent ions accelerated inwards at the front surface, ions accelerated at the rear surface, and the selection of ions escaping the simulating box within $10^{-4}$ srad solid angle around the rear surface normal.

*1. Ion acceleration at the front surface.*—First, we consider ion acceleration at the front boundary of the plasma and estimate the highest ion energy. A laser pulse incident at a sharp boundary of an overdense plasma exerts the ponderomotive force $e\langle c^{-1}\mathbf{v} \times \mathbf{B}_0\rangle$ on electrons in the skin layer. Here $\mathbf{v}$ is the electron quiver velocity in the laser field and $\mathbf{B}_0$ is the laser magnetic field. This force pushes electrons from their equilibrium positions into the plasma until it is balanced by the electrostatic field $E_s$ due to charge separation. We estimate the electrostatic field to be $eE_s/mc\omega_0 \approx a^2/2\sqrt{1 + a^2/2}$, where $a = eE/mc\omega_0$ is the usual dimensionless laser amplitude. This electrostatic field accelerates ions into the target and leads to hole boring in the overdense material [5,9]. The mean recession velocity $u_r$ can be estimated from momentum conservation [9], and in the case of total back reflection of the laser beam it is $(u_r/c)^2 = a^2mZn_c/Mn$, where $M$ is the ion mass, $Z$ is the ion charge, $n_c$ is the critical density for the laser beam, and $n$ is the electron density at the reflection point. If the plasma density is not sharp, but has some gradient, e.g., produced by the laser prepulse, the laser can propagate due to relativistically induced transparency [10] up to $n_r \approx n_c\sqrt{1 + a^2/2}$. The laser channels in the lower density regions [11] and the ions are accelerated mainly radially due to the channel Coulomb explosion [12,13]. Only at the density of $n_r$ the laser starts to push ions forward, and the recession velocity is the highest here, $(u_r/c)^2 \approx \sqrt{2}\, amZ/M$. The most energetic ions can acquire twice the recession velocity as they are bouncing in the potential well at the plasma boundary [14]. Thus, we expect the maximum energy of ions accelerated at the front surface of the target to be

$$E_{\max}^{\text{front}} \approx 2Mu_r^2 = 2\sqrt{2}\, aZ \times 0.511 \text{ MeV}. \qquad (1)$$

Here we have supposed $n = n_r$. Notice that the maximum ion energy depends only linearly on the laser amplitude. For the parameters of our simulation, formula (1) predicts $E_{\max} \approx 4.5$ MeV. The simulation—see Fig. 1—gives $E_{\max} \approx 3.5$ MeV for the ions at the front surface. The somewhat lower simulated energy is explained by finite absorption of the incident laser pulse.

The ions are accelerated down the gradient of the laser intensity. Thus, the angular directionality of ions accelerated at the front surface is defined by the particular pattern of the laser intensity distribution at the reflection position. In the case of a Gaussian beam with the waist $\sigma$, most of the ions should be accelerated within the laser focal cone $\alpha_f = \lambda/\sigma \approx 10^0$. In our simulation we observe the ions to be accelerated in a cone of about $20^0 \approx 2\alpha_f$, with some finer filamentory structure seen in Fig. 2(a). The large ion emission cone is due to the filamentory instability of the laser in the preplasma.

We do not observe any further energy gain of these ions as they propagate through the plasma bulk. In addition, the directionality of ions accelerated at the front surface is evidently defined by the laser intensity distribution, and not by the geometry of the rear target surface. The experiments, however, clearly demonstrate that the ions are emitted normally to the rear surface even for wedged targets [1,2]. This is strong evidence that the ion acceleration takes place at the rear surface; i.e., the second mechanism mentioned above is active. These ions have higher energies [1–3] than the estimation (1) for the simple laser ponderomotive push.

*2. Ions accelerated at the rear surface.*—The ions at the rear plasma surface are extracted by the space charge potential of the hot electrons. The problem of plasma expansion into vacuum has been studied a lot in planar geometry both theoretically and in experiments. Ion acceleration from the rear target surface has been observed even at laser intensities of $4 \times 10^{15}$ W/cm² [15]. The authors of [15] estimated the hot electron density at the rear surface
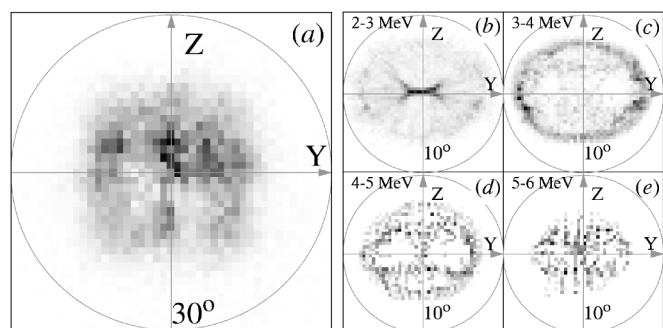


FIG. 2.   Angular distribution of ions. (a) The ions pushed into the foil at the plasma front surface. (b)–(e) Angular distribution of ions accelerated from the plasma rear surface within energy intervals: (b) 2–3 MeV; (c) 3–4 MeV; (d) 4–5 MeV; (e) 5–6 MeV.

and observed an anomalous stopping of the hot electrons as they propagate through targets of different thickness.

Analytical self-similar solutions for single-temperature isothermal or adiabatic plasma expansion have been obtained [16–18]. These solutions as well as numerical kinetic simulations [19] show that most of the ions are accelerated up to the electron thermal energy while ions in the high-energy tail of the distribution exceed this value several times. Recently, a set of three-dimensional self-similar solutions of plasma expansion into vacuum have been constructed [20].

In the case of short laser pulse interaction, there is not enough time to establish the thermal equilibrium in the plasma, and the electron distribution function is two-temperature-like. The lower temperature, $T^c$, corresponds to the bulk of background electrons, while a population of hot electrons heated directly by the laser has a much higher temperature $T^h$. The energy distribution of electrons in our simulation box at time $t = 660$ fs is shown in Fig. 3a as the filled circles. The hot electron temperature at this time is about $T^h \approx 2.6$ MeV. It is instructive to plot the spatial distributions of hot and cold electron populations. In Figs. 3b and 3c we show $X - Y$ cuts of the spatial distributions of electrons with energy below 100 keV (the "cold" population) and of those with energy above 100 keV (the "hots"). As we see, the cold electrons, Fig. 3b, stay within the original boundaries of the plasma layer while the hots, Fig. 3c, are exiting into vacuum and pull ions from the plasma rear surface.

Looking at the spatial distribution of the hot electrons, we see that even 100 laser periods after the pulse itself is over, the hot electrons still show a higher concentration along the laser axis in the middle of the plasma. We believe it is the self-generated magnetic field that confines the hot electrons here. As it has been shown earlier in [5,6], the beam of hot electrons generated at the front plasma surface is subject to Weibel instability when propagating through plasma [21,22]. The beam filaments and the spatial separation of the forward and return currents generates an azimuthal magnetic field. This field gets frozen into the plasma and remains even after the laser pulse is gone.
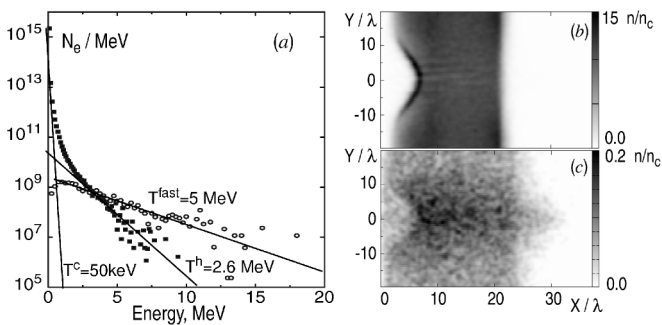
We do observe current filamentation and magnetic field generation in the present 3D PIC simulation. A 3D view of the static magnetic field is shown in Fig. 4a. The field is filamented inside the plasma. This multichannel magnetic structure guides the hot electrons through the plasma layer in a collimated way. When these collimated hot electrons exit into vacuum from the plasma rear surface, a "fountain" effect leads to the large-scale azimuthal magnetic field generation in the nearest vicinity of the surface. The generated magnetic fields are of the order of 10 MG. This is enough to collimate the hot electrons and influence directionality of the plasma expansion.

The strongest ion acceleration happens exactly in the middle of the magnetic torus produced by the fountain effect, as energies of the hot electrons and their density are the highest here. The plasma expansion takes the form of a conus with its peak at the fountain center. At the leading edge of the plasma expansion, the self-similar solutions do not hold anymore, as the Debye sheath is comparable with the plasma scale length here. At this low-density plasma front, the ions see the unscreened electric field of the electrons which are leaving the plasma. The ions in this sheath acquire the highest energies and form a peak at the very end of the ion energy spectrum [1,19,23]. The value of the electric field generated in the Debye sheath can be found from the Poisson equation for the electrostatic potential $\phi$:

$$\frac{e}{mc^2}\frac{d^2\phi}{dx^2} = \frac{n_0^h}{n_c}e^{e\phi/kT^h}, \qquad (2)$$

where $n_0^h$ is the hot electron density at the plasma boundary and $T^h$ is their effective temperature. We suppose that the hot electrons form a Boltzmann distribution in the potential. Integrating (2), we obtain the maximum electrostatic field $E_x$:

$$\frac{eE_x}{mc\omega_0} = \sqrt{2\,\frac{n_0^h T}{n_c mc^2}}. \qquad (3)$$



FIG. 3. (a) Energy spectrum of electrons in the simulation volume at time $t = 660$ fs displays two temperatures $T^c \approx 50$ keV and $T^h \approx 2.6$ MeV. (b) $X$-$Y$ density cut of cold electron population ($<100$ keV); (c) $X$-$Y$ density cut of hot electrons ($>100$ keV).
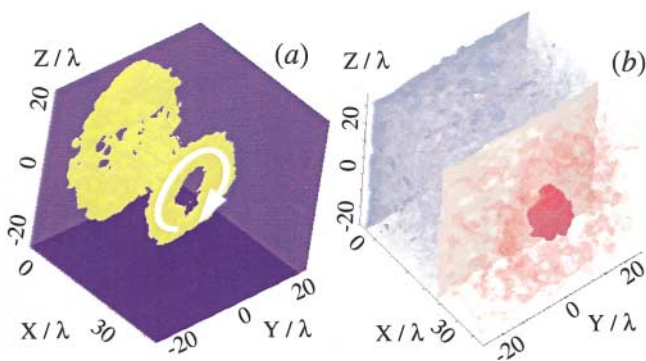


FIG. 4 (color). 3D perspective views. (a) Quasistatic magnetic field, the isosurface $|B| = 10$ MG is shown; the white arrow shows the field direction. (b) The accelerating electrostatic field $eE_x/mc\omega_0$, the isosurfaces have values: $-0.05$ (blue), 0.05 (light red); the dark red blob in the middle marks the Debye sheath with the highest electric field $eE_x/mc\omega_0 = 0.1$.

We do observe the unscreened electric field (3) in our 3D PIC simulations. It is seen as the dark red isosurface in Fig. 4b. This surface surrounds a region where the longitudinal electric field $E_x$ peaks. This is the Debye region of uncompensated charge.

The accelerating field $E_x$ has a pronounced three-dimensional structure. As a consequence, ions accelerated by this field have a corresponding angular distribution. In our simulation, we record information on all ions which exit the simulation box at the right boundary. Angular distributions of these ions in different energy ranges are shown in Figs. 2(b)–2(e). We observe some annular structures with radii decreasing as the energy of the ions increases. The rings have pretty sharp outer boundaries.

We should mention here that similar ring structures in ion angular distributions have been observed by the Rutherford group [3], when they shot on relatively thin foils, about 50 $\mu$m thick. At the same time, experiments with 1 mm thick targets at the PetaWatt laser at LLNL [1,2] show energetic ions emerging in filled circles with a smooth outer boundary. Though we cannot simulate 1 mm thick solid density targets with our 3D PIC code at the moment, we conjecture that the difference is due to the different regimes of hot electron propagation in these experiments. The magnetic channels we observe, Fig. 4a, need a finite time to be formed. Their formation starts at the front plasma surface and the channels are continuously elongating into the plasma bulk at the speed of about $c/4$ in this simulation, as long as the laser is on. Thus, if the target is too thick, the channels simply do not have time to reach the rear surface. The hot electrons would be unmagnetized then and spray over the full target. The toroidal magnetic field at the rear plasma surface would be absent, and the plasma expansion is quasi one dimensional. The maximum ion energies in this case are defined by electron thermal velocities and can be very high, as the experiment [1,2,15] and 1D PIC simulations [19] show.

In conclusion, we have used the 3D PIC code VLPL to simulate a model problem of ion acceleration in laser interaction with overdense plasma layers, paying particular attention to the ions emerging from the rear surfaces of the plasma. Though we observe ion acceleration both at the front and the rear plasma surfaces, we find that ion acceleration from the front surface can hardly explain energies and directionality of the ion beams detected in recent experiments [1–3]. These "front" ions have relatively low energies (1) and are emitted in a large solid angle. At the same time, ions pulled out from the rear surface by the space charge potential of hot electrons are highly directed and may account for the experimental observations. In our simulation with relatively thin plasma layers, we observe a ringlike angular distribution of the energetic ions resembling that detected in the experiment [3]. We attribute these ring structures to the 3D shape of the electrostatic field induced in the Debye sheath at the leading edge of the expanding plasma.

One of the key parameters influencing the Debye sheath and the ion acceleration is the density scale length at the rear surface. Here we have used a steep, 0.5 $\mu$m, density scale. The detailed investigation of ion beam characteristics as the function of the plasma scale length will be published elsewhere.

[1] S. Hatchett *et al.,* Phys. Plasmas **7**, 2076 (2000).
[2] R. A. Snavely *et al.,* Phys. Rev. Lett. **85**, 2945 (2000).
[3] E. L. Clark *et al.,* Phys. Rev. Lett. **84**, 670 (2000); K. Krushelnik *et al.,* Phys. Plasmas **7**, 2055 (2000).
[4] M. Roth *et al.,* Phys. Rev. Lett. **86**, 436 (2001).
[5] A. Pukhov and J. Meyer-ter-Vehn, Phys. Rev. Lett. **79**, 2686 (1997).
[6] M. Honda, J. Meyer-ter-Vehn, and A. Pukhov, Phys. Plasmas **7**, 1302 (2000).
[7] J. Davies *et al.,* Phys. Rev. E **56**, 7193 (1997).
[8] A. Pukhov, J. Plasma Phys. **61**, 425 (1999).
[9] S. C. Wilks, W. L. Kruer, M. Tabak, and A. B. Langdon, Phys. Rev. Lett. **69**, 1383 (1992).
[10] E. Lefebvre and G. Bonnaud, Phys. Rev. Lett. **74**, 2002 (1995).
[11] A. Pukhov and J. Meyer-ter-Vehn, Phys. Rev. Lett. **76**, 3975 (1996).
[12] A. Pukhov, Z.-M. Sheng, and J. Meyer-ter-Vehn, Phys. Plasmas **6**, 2847 (1999).
[13] G. Pretzler *et al.,* Phys. Rev. E **58**, 1165 (1998).
[14] J. Denavit, Phys. Rev. Lett. **69**, 3052 (1992).
[15] G. D. Tsakiris *et al.,* Phys. Rev. Lett. **46**, 1202 (1981).
[16] W. Kruer, *The Physics of Laser-Plasma Interactions* (Addison-Wesley, Reading, MA, 1988).
[17] A. Gurevich, D. Anderson, and H. Wilhelmsson, Phys. Rev. Lett. **42**, 769 (1979).
[18] P. Mora and R. Pellat, Phys. Fluids **22**, 2300 (1979).
[19] J. Denavit, Phys. Fluids **22**, 1384 (1979).
[20] D. S. Dorozhkina and V. E. Semenov, JETP Lett. **67**, 573 (1998).
[21] E. S. Weibel, Phys. Rev. Lett. **2**, 83 (1959).
[22] F. Califano *et al.,* Phys. Rev. E **58**, 7837 (1998).
[23] Ch. Sack and H. Schamel, Phys. Rep. **156**, 311 (1987).